Since January 2020 Elsevier has created a COVID-19 resource centre with free information in English and Mandarin on the novel coronavirus COVID-19. The COVID-19 resource centre is hosted on Elsevier Connect, the company's public news and information website.

Elsevier hereby grants permission to make all its COVID-19-related research that is available on the COVID-19 resource centre - including this research content - immediately available in PubMed Central and other publicly funded repositories, such as the WHO COVID database with rights for unrestricted research re-use and analyses in any form or by any means with acknowledgement of the original source. These permissions are granted for free by Elsevier for as long as the COVID-19 resource centre remains active.

CARBON 75 (2014) 401–410

Available at www.sciencedirect.com

ScienceDirect

journal homepage: www.elsevier.com/locate/carbon

Filtration and inactivation of aerosolized bacteriophage MS2 by a CNT air filter fabricated using electro-aerodynamic deposition

Kyu-Tae Park, Jungho Hwang *

Mechanical Engineering Department, Yonsei University, Seoul, Republic of Korea

ARTICLE INFO

Article history:
Received 15 January 2014
Accepted 3 April 2014
Available online 13 April 2014

ABSTRACT

Carbon nanotubes (CNTs) were coated on a sample of glass fiber air filter medium at atmospheric pressure and room temperature using electro-aerodynamic deposition (EAD). In the EAD method, CNTs (diameter: 50 nm, length: 2–3 μm) were aerosolized, electrically charged, and injected through a nozzle. A voltage was applied externally between the ground nozzle and a planar electrode on which the sample was located. The charged CNTs were deposited on the sample in a vertically standing posture even at a low flow velocity. Before the deposition experiment, a calculation was performed to determine the applied voltage by simulating the electric field, flow field, and particle trajectory. Using CNT-coated filter samples, virus aerosol filtration and anti-viral tests were carried out using the aerosol number counting method and the plaque counting method, respectively. For this purpose, bacteriophage MS2 was aerosolized with an atomizer. The particle filtration efficiency was increased to 33.3% in the most penetration particle size zone (100 nm) and the antiviral efficiency of the CNT filter was 92% when the coating areal density was 1.5×10^9 #/cm^2. The susceptibility constant of virus to CNTs was 0.2 cm^2/μg.

© 2014 Elsevier Ltd. All rights reserved.

1. Introduction

Biological aerosols generally include bacteria, fungi, viruses and their derivatives such as endotoxin, glucans and mycotoxin. Exposure has been shown to cause many adverse health effects including allergic, toxic, and infectious responses [1–3]. Aerosol transmission is known to play an important role in observed airborne microbial infections. Studies indicate that large scale outbreaks of severe acute respiratory syndrome (SARS) were mainly the result of airborne exposure routes [4,5]. Viruses are detected in air samples collected from hospital rooms [6,7] and also in human breath [8,9]. A study indicated that there was an approximately 23% possibility of influenza virus infections in people wearing surgical and N95 respiratory masks [10]. Therefore, development of efficient air control technology is important in combating inhalation-related diseases.

Over the years, a large volume of studies have been undertaken to develop air cleaning technologies. Among the various air cleaning techniques, filtration is widely applied to remove particles from air streams. However, recent research has demonstrated that some microorganisms are capable of colonizing the air filter surface in heating, ventilating, and air-conditioning systems (HVAC) [11–13], and the organic or inorganic materials deposited on the filter surface can contribute to microbial growth. Air filters contaminated by microorganisms lead to the release of microorganisms from the filter surface [14], and the emission of volatile organic

* *Corresponding author:* Fax: +82 2 312 2821.
E-mail address: hwangjh@yonsei.ac.kr (J. Hwang).
http://dx.doi.org/10.1016/j.carbon.2014.04.019
0008-6223/© 2014 Elsevier Ltd. All rights reserved.

compounds (VOCs) produced by microbial metabolism [11,12]. Biologically contaminated filter could pose a significant health hazard through reaerosolizing opportunistic pathogenic or allergenic aerosols [15]. Antimicrobial treatment could be a possible solution to these problems.

Carbon nanotubes (CNTs) have been increasingly used in environmental applications due to their high specific surface area, smooth surface, and adsorption capability [16]. Recently, multi-walled and single-walled CNT filters were developed and found to be effective for multilog microbial removal from contaminated water by physical straining, puncture and depth filtration [17–20]. CNTs were shown to inactivate the highest percentage of cells both in monocultures and diverse microbial communities of river water and wastewater effluents [21–23]. A CNT filter was successfully created and utilized to remove biological agents from water with filtration efficiency [17–21,24–26].

Even though carbon nanotube filters have been extensively studied for water purification, there are only a few reports in the literature on carbon nanotube use for air purification. Viswanathan et al. [27] presented the first investigation of the use of multi-walled carbon nanotubes (MWCNTs) as high efficient, airborne particulate filter media. High filtration efficiencies were achieved from films of MWCNTs deposited onto cellulose fiber filters. The MWCNT-coated filters exhibited low pressure drops and better filter quality than cellulose filters. Park and Lee [28] constructed a metal MWCNT filter in which carbon nanotubes were grown directly on the micron-sized metallic fibers of the air filter using the thermal chemical vapor deposition (CVD) method. The metal MWCNT filter had higher filtration efficiency than conventional filters without a significant decrease in pressure. Karwa and Tatarcuk [29] studied an enhancement in aerosol filtration by synthesizing carbon nanostructures including nanofibers within nickel sintered metal microfibrous matrices/filter media. Their study showed that carbon nanostructure synthesis led to significant improvement in the performance of filter media with large initial pore size because the pore diameters did not reduce significantly with synthesis. Yildiz and Bradford [30] prepared novel filters by drawing aligned CNTs sheets and embedding them between polypropylene melt-blown nonwoven fabrics using calendaring. The filters were prepared with an increasing number of CNT sheets. The filtration performance of the novel filters showed that when the number of CNTs layers increased, the filtration efficiency increased dramatically, while the pressure drop also increased. Guan and Yao [31] investigated the removal efficiencies of CNT filters for a collection of aerosolized biological and non-biological particles. In their preparation of the CNT filters, a predetermined volume of CNT suspension with a certain concentration was uniformly filtered through the membrane support. The removal efficiencies for aerosols and bacteria were shown to increase with increased loadings of CNTs regardless of membrane supports and pore size tested. Xu and Yao [32] fabricated a single walled carbon nanotube (SWCNT) filter with CNT solution, and investigated its anti-bacterial efficacy with CNT loading. Their results revealed that particle types and CNT loading had greater effects on anti-bacterial efficacy than other membrane types and pore sizes tested. Park et al. [33] reported that a MWCNT-deposited glass fiber filter showed increased particle filtration efficiency and antibacterial activity. In the fabrication of CNT filters, samples of glass fiber filter media were catalytically activated with iron (Fe) nanoparticles generated by the spark discharge method. The catalytically activated filter samples were placed in a thermal CVD reactor in which MWCNT fibers were vertically grown on the activated spots after acetylene (C_2H_2) gas was carried into the reactor.

However, the fabrication of a CNT filter using the spark discharge method followed by the CVD process requires time and effort in controlling the operation of a CVD reactor. In addition, the durability of a CNT filter made by the CVD process can be degraded in the high temperature environment associated with the CVD process. In this paper, we suggest an aerosol process of fabricating a CNT filter at atmospheric pressure and temperature using the electro-aerodynamic deposition (EAD) method, the details of which were introduced in our previous study [34]. In the EAD method, CNTs were aerosolized, electrically charged, and injected through a nozzle, where an external electric field was applied. The charged CNTs were vertically deposited on the glass fiber filter media even at a low flow velocity. Using CNT coated filter samples, virus aerosol filtration and anti-viral tests were carried out using the aerosol number counting technique and the plaque counting method, respectively.

Susceptibility has been used to explain the relative importance of various parameters affecting antimicrobial efficacy. Yoon et al. [35] used susceptibility to evaluate the antibacterial effects of silver and copper nanoparticles. Kim et al. [36] applied susceptibility to evaluate the antibacterial effects of corona discharge-generated ions in the air. In this paper, the susceptibility of a virus to CNTs was calculated to determine the inactivation efficacy with respect to CNT concentration.

2. Materials and methods

2.1. CNT filter fabrication

Fig. 1 shows the process of coating CNTs on a substrate. The set-up consisted of CNT aerosolization (A), CNT charging (B), and CNT deposition (C) equipment. Commercial MWCNTs (Nanokarbon, Korea) with a diameter of 50 nm and a length of 2–3 μm were used. After compressed air was passed through a clean air supply consisting of an oil trap, diffusion dryer, and high efficiency particulate air (HEPA) filter, the particle-free compressed air entered a Collison type atomizer (9302, TSI Inc., USA), which was filled with 9 ml of de-ionized water and 1 ml of 1% CNT solution. The aerosol flow rate was controlled by a rotameter. Dry, clean air at 3 lpm formed a high-velocity jet through an orifice in the atomizer. The pressure drop from this jet drew the CNT solution up through a tube. The solution was then broken up into droplets by the high-velocity air jet. The resultant larger droplets impinged on an impactor, while the smaller droplets made no contact and formed an aerosol that exited through an outlet. The aerosolized CNTs were passed through a diffusion dryer for water removal and a neutralizer (Soft X-ray charger 4530,

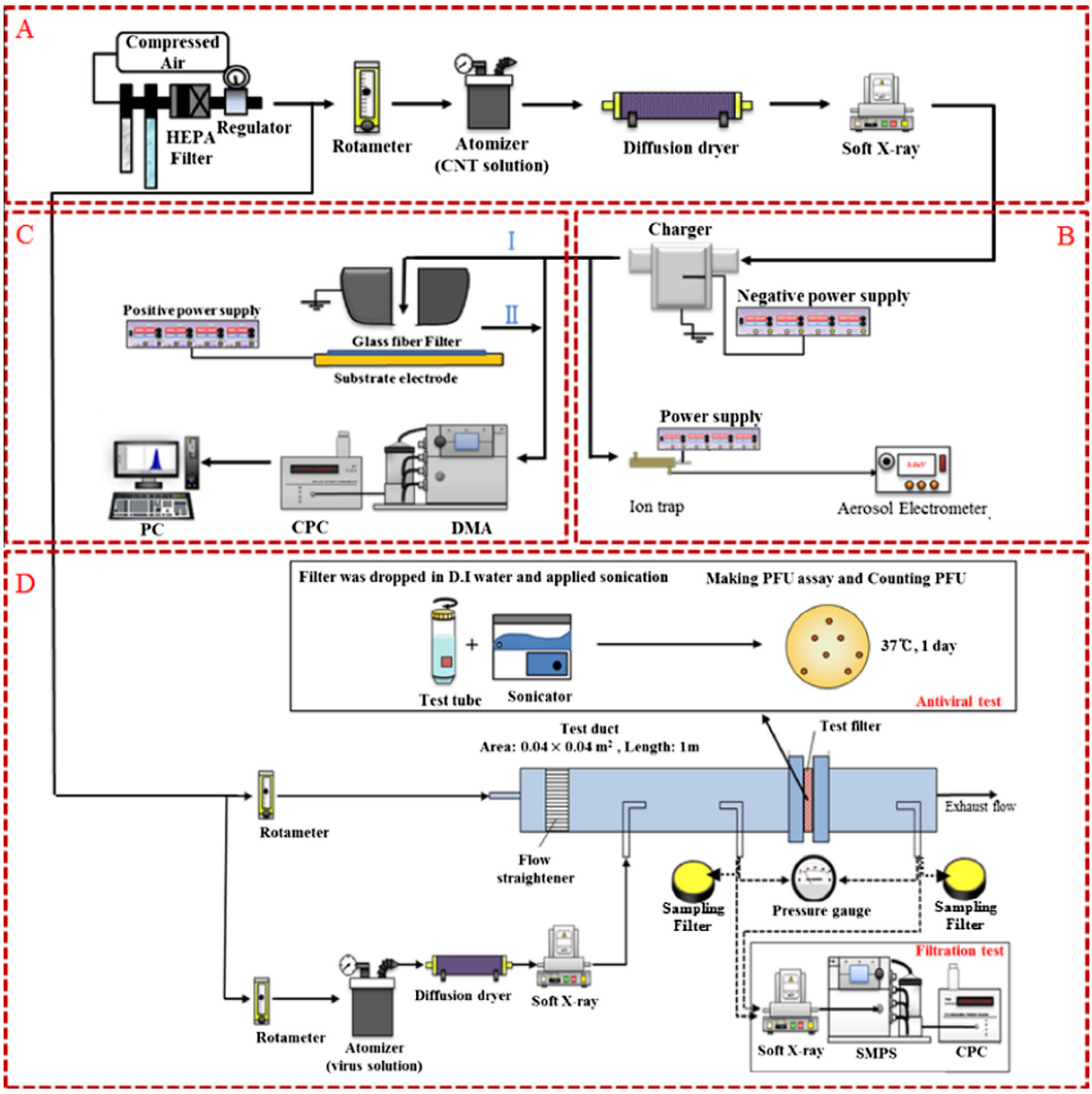

Fig. 1 – Schematic of the electro-aerodynamic deposition system used for CNT filter fabrication (A, B, C) and experimental setup (D) for filtration, pressure drop, and antiviral tests. (A color version of this figure can be viewed online.)

HCT, Korea) to induce a Boltzmann charge distribution (Fig. 1(A)).

The neutralized CNTs entered a unipolar charger where a stainless steel needle (wire) electrode, located at the center, was used to generate a corona discharge on its sharp tip (Fig. 1B). The corona discharge generated air ions, which moved along the electric field to a grounded cylinder (made of Duralumin). The amount of charge per particle was controlled by DC voltage supplied from a high voltage power supply. A voltage of −8 kV was applied to the needle to charge the CNTs. Details of the charger are described in Park et al. [37].

The electrical current carried by the charged CNTs was measured with an aerosol electrometer (3068A, TSI, ISA) to obtain the average charge number of the CNTs, using the following equation:

$$n_p = \frac{I}{N \cdot e \cdot Q} \quad (1)$$

where n_p is the average charge number, e is the elementary charge, I is the measured current, Q is the flow rate, and N is the number concentration of the charged CNTs (Fig. 1B). An ion trap was used to remove free unattached ions and allow charged particles to pass through the ion trap zone. The ion trap voltage was 200 V [38].

The charged CNTs then entered a cylindrical nozzle (Fig. 1C) with a length of 30 cm and a diameter of 6 mm, which induced a fully developed flow and minimize the entrance effect at the nozzle (Re = 700). The nozzle filet had a finite radius of curvature (2 mm) at the tip so that the electric field applied to this tip was minimized [39]. After the charged CNTs were ejected from the nozzle, they were guided

by electrical force to deposit on a substrate located on an electrode to which a high voltage was applied. The distance between the nozzle and the substrate was 10 mm. A silicon wafer or glass fiber filter medium (Fabriano, Italy) was used as the substrate.

Before the deposition experiment, a calculation was performed to determine the voltage applied to the substrate. Commercial computational fluid dynamics (CFD) software, FLUENT, with external user defined function (UDF) code was used to simulate the electric field, flow field, and particle charging motion. FLUENT is a solver software package for various physics and engineering applications and utilizes the finite volume method (FVM). Even though FLUENT does not include an electric field solver, UDFs allow for the customization of FLUENT to fit particular modeling needs. The discrete phase model (DPM) and the Laminar model in FLUENT were used as the particle solver and the flow solver, respectively.

First, the continuity equation and Navier–Stokes equation were solved for the flow velocity. The electric field was then obtained by solving Poisson's equation with known particle concentration and particle charge (n_p) values. Finally, the particle trajectory was calculated using the following equation:

$$\frac{d\vec{u}_p}{dt} = \frac{18\mu}{d_p^2 \rho_p C_c}(\vec{u} - \vec{u_p}) + \frac{\vec{g}(\rho_p - \rho)}{\rho_p} + \vec{F}_p \quad (2)$$

where $\vec{u}$ is the flow velocity, ρ is the density of air, $\vec{g}$ is the gravitational constant, d_p is the particle diameter, $\vec{u}_p$ is the particle velocity, ρ_p is the particle density, C_c is the Cunningham slip correction factor, and μ is the dynamic viscosity of air. $\vec{F}_p$ in Eq. (2) describes the electrostatic forces on a particle (per unit mass) and can be expressed as follows:

$$\vec{F}_p = \vec{F}_E + \vec{F}_{Di} + \vec{F}_{Im} \quad (3)$$

where $\vec{F}_E$ is the Coulombic force per unit mass that is induced by charges and electric fields, $\vec{F}_{Di}$ is the dipole force per unit mass, and $\vec{F}_{Im}$ is the image force acting on a particle per unit mass [40,41]. Simulation details can be found in Park et al. [34].

A scanning mobility particle sizer (SMPS) system consisting of a differential mobility analyzer (DMA, 3081, TSI, USA) and a condensation particle counter (CPC, 3025, TSI, USA) was utilized to evaluate the CNT coating efficiency (Fig. 1C). Aerosol sampling was carried out upstream of the nozzle (I) and also at the air outlet (II) from undeposited CNTs exited. The SMPS system was operated under a sampling flow rate of 0.3 lpm and a scan time of 180 s.

After fabrication of the CNT filter using glass fiber filter medium as the substrate, it was necessary to confirm whether the CNTs were firmly deposited on the glass fibers. For this purpose, clean air with a face velocity of 1.5 m/s was forced to flow through the CNT filter. A SMPS was located downstream of the CNT filter to measure the number of CNTs that detached from the filter.

2.2. Preparation of virus solution

Bacteriophage MS2 (ATCC 15597-B1) and *Escherichia coli* strain C3000 (ATTCC 15597) were selected as the test virus and host bacteria, respectively. To recover bacterial cells from a freeze-dried state, 10 ml of tryptic soy broth (TSB) was mixed with the freeze-dried bacterial cells and the mixture was incubated with shaking for 24 h at 37 °C. A total of 0.1 ml of the incubated bacterial solution was injected into the 10 ml of TSB. The TSB solution containing the bacteria was used as the host bacterial solution after incubation with shaking for six hours at 37 °C.

One milliliter of TSB was injected into the freeze-dried MS2 virus, and 0.1 ml of the viral solution was extracted. The extracted solution was mixed with 0.3 ml of the host bacterial solution and 29 ml of soft tryptic soy agar (TSA) containing 8 g/l of agar. The resulting agar solution was poured into a Petri dish and incubated overnight at 37 °C. The surface of the agar was scraped off with 10 ml of phosphate buffer solution (PBS), pH 7.0. The solution was centrifuged for 20 min at 5000G, and the supernatant was used as the virus solution in subsequent experiments.

2.3. Filtration test

Prior to filtration testing, the pressure drop across the CNT filter was measured using a differential pressure gauge (Magnehelic 2000, Dwyer Instruments Inc., USA) with various face velocities of clean air ranging from 0.0 m/s to 0.2 m/s.

After the pressure drop test, the filtration test was carried out using bacteriophage MS2. The experimental setup for the filtration test is shown in Fig. 1D. The system consisted of a test duct with a cross-sectional area of 40 mm × 40 mm and a length of 1000 mm, a test particle generation system, and a measurement system. A CNT filter sample was installed in the middle of the test duct. Two isokinetic stainless steel sampling probes were placed before and after the filter media for aerosol sampling. Aerosolized virus particles were supplied to the test duct by the same procedure used in the supply of aerosolized CNTs. The number concentration of the virus particles was measured using an SMPS before and after the filter. A stream of clean air was delivered to the test duct and mixed with the particle-laden air flow to adjust the flow velocity. The fractional particle filtration efficiency, $\eta_F(d_p)$, was defined using the following equation:

$$\eta_F(d_p) = 1 - \frac{C_{downstream}(d_p)}{C_{upstream}(d_p)} \quad (4)$$

where $C(d_p)$ is the number concentration of aerosolized bacteriophage MS2 of size d_p. The filter quality factor was evaluated with various face velocities using following equation:

$$q_F = \frac{\ln\left(\frac{1}{1-\eta_F}\right)}{\Delta p} \quad (5)$$

where q_F is the quality factor, Δp is the pressure drop, and η_F is the integrated value of $\eta_F(d_p)$ over the particle size d_p.

2.4. Antiviral test

The experimental set-up for the antiviral test is also shown in Fig. 1D. To aerosolize the virus particles, 0.1 ml of the supernatant was diluted with 50 ml deionized (DI) water. The virus particles were aerosolized, and deposited onto each test filter for 30 min in the test duct. A pristine filter and CNT-coated filter were used for comparison. Each filter was put into the 10 ml of DI water and subjected to sonication for ten minutes

with a batch-type sonicator (KMC1300V, Vision Scientific, Korea) to detach deposited virus particles from the filter. Then 0.1 ml of the water containing virus particles was mixed with 0.3 ml of host bacterial solution and 29 ml of soft TSA. The mixed solution was poured into a Petri dish and incubated overnight at 37 °C. The number of plaques that appeared on the plate was counted and the antiviral efficiency was calculated using the following equation:

$$\eta_A = 1 - \frac{PFU_{CNT\ filter}}{PFU_{Pristine\ filter}} \quad (6)$$

where the numerator is the number of plaque forming units (PFU) on the nutrient agar plate after incubation when the CNT filter was used, and the denominator is the number of plaque forming units on the nutrient agar plate after incubation when the pristine glass fiber filter was used.

The susceptibility of virus to CNTs was determined by calculating the susceptibility constant Z defined by the following equation,

$$Z = \frac{-\ln(1-\eta_A)}{C} \quad (7)$$

where C is the coating areal mass density of CNTs (μg/cm^2). A higher Z value implies higher antiviral activity. Moreover, experiments were carried out to compare the viable viral count in the air before and after the filtration, with both pristine and modified filters under the same experimental condition with the filtration test (at face velocity: 0.2 m/s). We generated virus with an atomizer and sampled aerosolized virus at both upstream and downstream the test filter. The sampled virus was captured on a sampling filter and cultured for PFU counting.

3. Results and discussion

3.1. Fabrication of CNT filter

The process depositing of CNTs on a glass fiber filter sample required that the CNTs were highly charged by the corona charger. When a voltage of −8 kV was applied to the needle of the charger, the current carried by the charged CNTs was measured to estimate their average charge using Eq. (1). With measured values of I (=3.6×10^{-12} A), Q (=3 lpm), and N (=4.52×10^{5} #/cm^3), we determined that the average charge number was 110, which was in good agreement with the value of 116 obtained from calculation using the classical charging theory [40]. In the calculation, we assumed that the CNTs had a shape factor of 1.91 [40]. The particle diameter calculated with this shape factor was 162 nm, which was very close to 160 nm measured using the SMPS system.

For a given CNT charge number, a calculation was carried out to determine the voltage applied to the substrate. Fig. 2 shows the (a) voltage distribution and (b) trajectories of CNTs near the substrate, under the electric field. When the applied voltage was less than 300 V, CNT particles would not deposit on the substrate. However, at a potential of 300 V, CNTs started to deposit on the substrate and the CNT deposition area decreased. The calculated results were in good agreement with those predicted by the following equation [34]:

$$\frac{W_p}{W} \cong 0.96\left(\frac{n_p e C_c V}{3\pi\mu U d_p h}\right)^{-0.41} \quad (8)$$

where W is the nozzle width, U is the flow velocity at the nozzle, V is the voltage applied to the substrate, h is the distance between the nozzle and the substrate, and W_p is the radius of the coated region.

CNT deposition experiments were conducted with a Si wafer substrate. Fig. 3 shows field emission scanning electron microscopy (FE-SEM) images of CNTs deposited on the substrate. When the charger was not operated, there were no CNTs observed on the substrate, regardless of the voltage applied (Fig. 3(a)). When charged CNTs were flowing toward the substrate where no electric field was applied, several particles were deposited as shown in Fig. 3(b), which was caused by an image force between the CNTs and the substrate (Eq. (3)). When the charged CNTs were delivered to a substrate of opposite polarity, many of them were successfully deposited on the

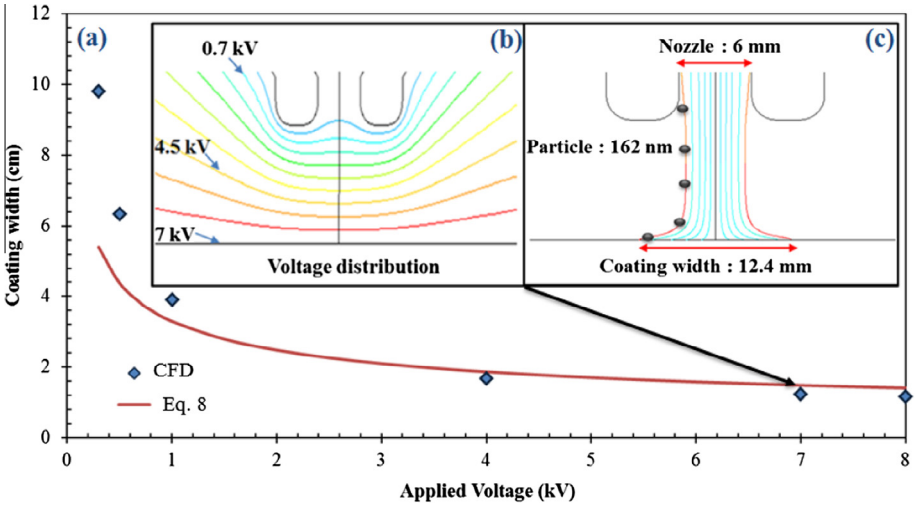

Fig. 2 – (a) Effect of applied voltage on the CNT coating width. (b) Spatial voltage distribution between the nozzle and the substrate (applied voltage of 7 kV). (c) Particle trajectory and coating width (applied voltage of 7 kV). (A color version of this figure can be viewed online.)

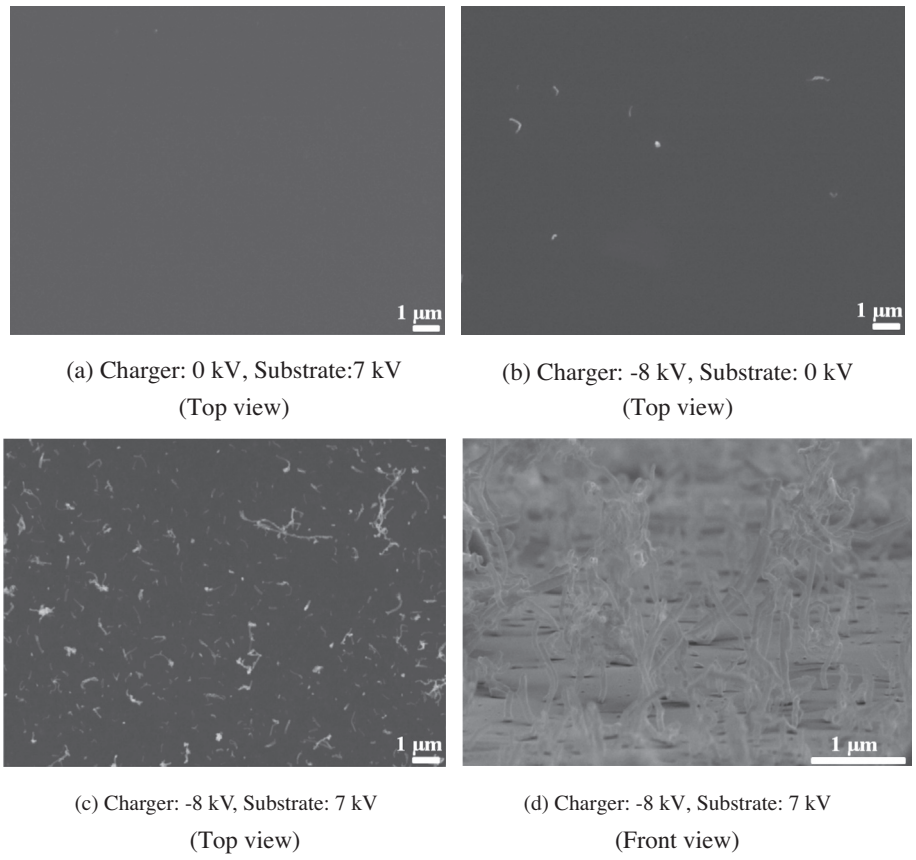

(a) Charger: 0 kV, Substrate:7 kV (Top view)

(b) Charger: -8 kV, Substrate: 0 kV (Top view)

(c) Charger: -8 kV, Substrate: 7 kV (Top view)

(d) Charger: -8 kV, Substrate: 7 kV (Front view)

Fig. 3 – FE-SEM images of CNT deposition under various conditions.

surface (Fig. 3(c)). Fig. 3(d) shows a frontal view of the deposited CNTs. Note that the CNTs were vertically aligned. This phenomenon was due to characteristics of the charged CNTs. According to Keblinski et al. [42], CNTs have higher charge concentration on both tube ends than in the central part. Therefore, when they landed on the substrate the end of each CNT that was closer to the substrate than the other end was attracted to the substrate, resulting in the standing posture of the tubes.

The CNT deposition experiment was also carried out using glass fiber filter medium as the substrate. The cross-sectional size of the filter was 40 mm × 40 mm. Fig. 4 shows the size distribution of CNTs measured before the nozzle inlet (location I in Fig. 1) and away from the nozzle outlet (II), measured with the SMPS system. The total number concentrations of CNTs at locations I and II were 4.52×10^5 #/cm^3 and 7.5×10^3 #/cm^3, respectively, resulting in a coating efficiency of 83%. With coating times of 3 min, 5 min, and 10 min, the coating areal densities of fabricated CNT filters were 4.5×10^8 #/cm^2, 7.5×10^8 #/cm^2, and 1.5×10^9 #/cm^2, respectively. Fig. 5 shows an FE-SEM image of the CNT-coated filter (coating time = 3 min). The CNTs were observed to be standing vertically on each filter fiber.

Experiments were carried out using forced clean air with a face velocity of 1.5 m/s in order to determine whether CNTs could be detached from the filter. The results in Fig. 6(a) show that no CNTs were detached from any of the three filter samples. The pressure drop across each test filter media was also

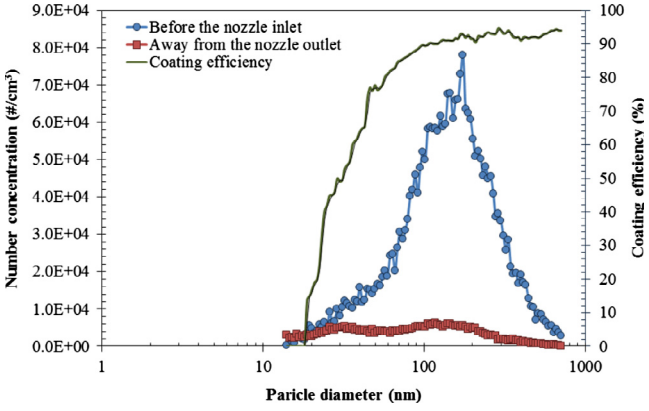

Fig. 4 – CNT coating efficiency. (A color version of this figure can be viewed online.)

measured at various face velocities of the clean air. The results are summarized in Fig. 6(b), which shows that CNT deposition did not affect the pressure drop, implying that the change in filter solidity due to the addition of the CNTs was negligible. For comparison, the following theoretical prediction of pressure drop was used [43]:

$$\Delta p = \frac{64\mu t U_0 \alpha^{1.5}(1 + 56\alpha^3)}{d_f^2} \quad (9)$$

where, U_0 is the face velocity, t is the filter thickness (=0.2 mm), α is the solidity (=0.11), and d_f is the diameter of

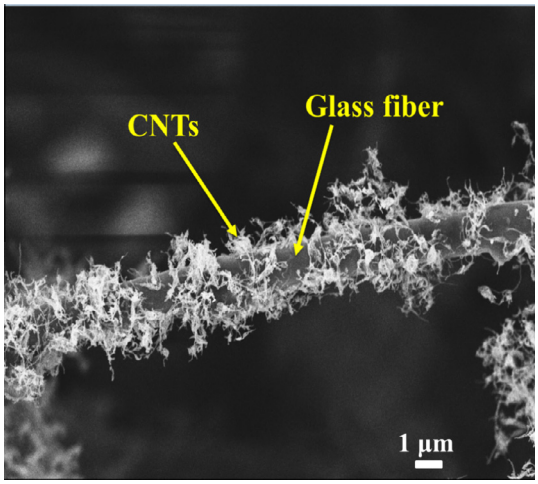

Fig. 5 – FE-SEM images of the CNT-coated filter. (A color version of this figure can be viewed online.)

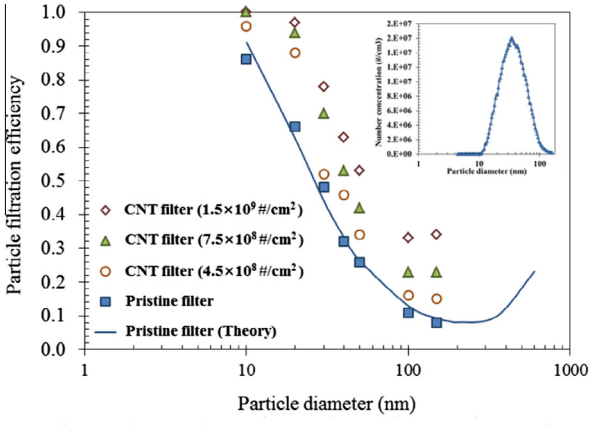

Fig. 7 – Filtration of viral particles. (A color version of this figure can be viewed online.)

filter fiber (=4 μm). The calculations were consistent with the data from the pristine test filter.

3.2. *Filtration test*

The size distribution of the aerosolized viral particles (bacteriophage MS2) is shown in the inset of Fig. 7. The total concentration and mode diameter were 8.6×10^6 #/cm^3 and 37.2 nm, respectively. Fig. 7 shows the effect of CNT coating on filtration efficiency as a function of particle diameter ($\eta_F(d_p)$). The face velocity was 0.2 m/s. The results show that the filtration efficiency was improved overall by the presence of CNTs on the glass fiber filter. The overall filtration efficiencies (η_F) were 54%, 66.2%, 70%, and 78.4% for the pristine filter and CNT filters with coating areal densities of 4.5×10^8 #/cm^2, 7.5×10^8 #/cm^2, and 1.5×10^9 #/cm^2, respectively. Particle sizes of 120 nm and 100 nm were the most abundant penetration particle size for the pristine filter and CNT-coated filter, respectively. The fractional filtration efficiency was 11% (d_p = 120 nm) with the pristine filter, but increased to 33.3% (d_p = 100 nm) with the CNT-coated filter (coating areal density: 1.5×10^9 #/cm^2). For the pristine filter, the fractional filtration efficiency was also determined theoretically using the following equation [22]:

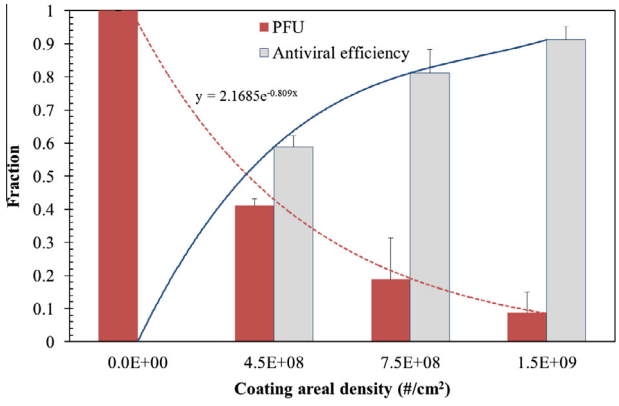

Fig. 8 – Antiviral test results. (A color version of this figure can be viewed online.)

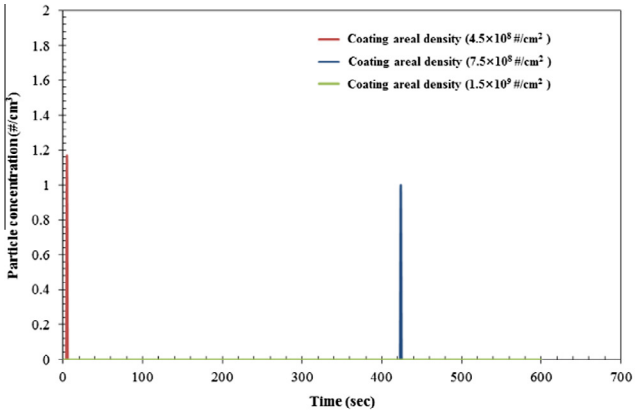

(a) Detachment test

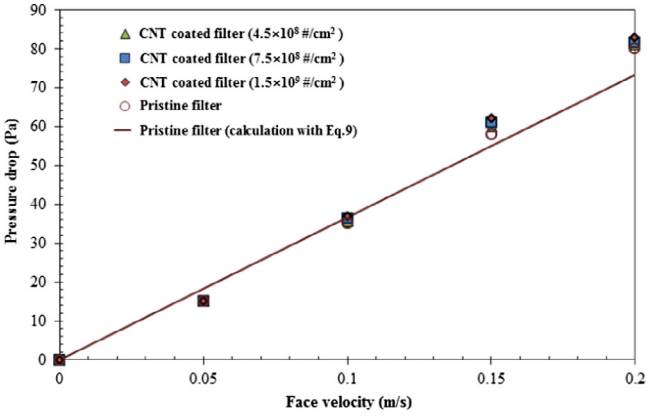

(b) Pressure drop test

Fig. 6 – Experimental results. (A color version of this figure can be viewed online.)

$$\eta_p(d_p) = 1 - \exp\left[-\frac{4\alpha t E(d_p)}{\pi d_f(1-\alpha)}\right] \quad (10)$$

The single fiber (fractional) filtration efficiency $E(d_p)$ is defined as

$$E(d_p) = 1 - (1 - E_{diff}(d_p)) \times (1 - E_{int}(d_p)) \times (1 - E_{imp}(d_p)) \quad (11)$$

where E_{diff}, E_{int}, and E_{imp} are the filtration efficiencies due to Brownian diffusion, interception, and inertial impaction, respectively [40]. The theoretical results were in good agreement with the experimental data.

Quality factors were evaluated using Eq. (5) for various face velocities. The quality factor increased with coating areal density for a given face velocity, but decreased with face velocity for a given coating areal density. The best quality factor of 0.13 (44% increase compared to the pristine filter) was obtained when the face velocity was 0.05 m/s and the coating areal density was 1.5×10^9 #/cm^2.

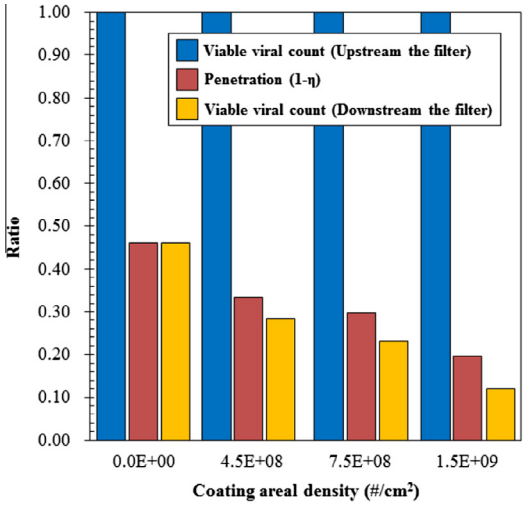

Fig. 9 – Viable viral count ratios before and after filtration. (A color version of this figure can be viewed online.)

3.3. *Antiviral efficiency*

Fig. 8 shows the results of antiviral testing. As the coating areal density increased, the PFU value decreased exponentially (decay constant = −0.809 cm^2). The filter had higher antiviral efficiency with increasing CNT density. The antiviral efficiency was 92% with a coating areal density of 1.5×10^9 #/cm^2. The relationship between $-\ln(1-\eta_A)$ and C is the Z value, which is the slope of the line, was 0.1944 cm^2/μg.

According to Fig. 9, the viable viral count ratio in the air before and after the filtration for a pristine filter (coating areal density = 0) was same as the penetration ratio ($1-\eta_F$). However, in case of CNT coated filters, the viable viral count ratio was lower than the penetration ratio and decreased with coating areal density, implicating that the virus could be physically damaged when they passed through the CNT coated filter.

Fig. 10(a) shows TEM images of viruses sampled from the viral solution which was prepared by filtration of the viruses on the pristine filter and subsequent detachment of the viruses from the pristine filter with sonication in de-ionized water. Their shape was close to circular with a diameter of approximately 40 nm, which was consistent with the value measured using the SMPS as shown in the inset of Fig. 7. Fig. 10(b) and (c) shows TEM images of viruses captured on the CNTs. Fig. 10(b) and (c) also shows viruses that were detached from the CNTs during the sonication process. The

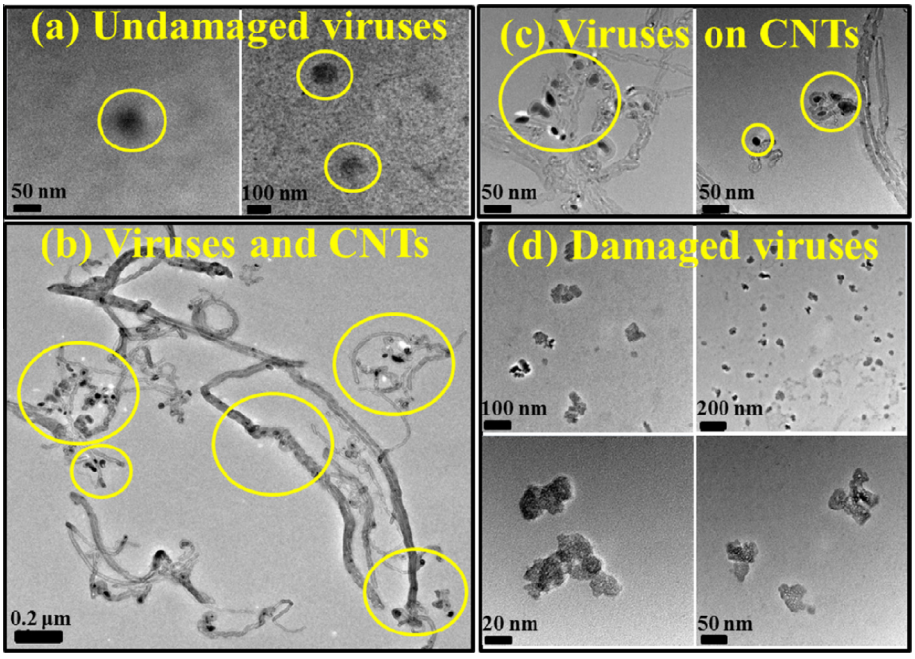

Fig. 10 – (a) Viruses detached from the pristine filter. (b) and (c) TEM images of CNTs and viruses captured on the CNTs. (d) Damaged viruses. (A color version of this figure can be viewed online.)

morphology of the detached viruses changed to a dumbbell-like or tore shape, clearly seen in Fig. 10(d).

In previous studies [17–20], viruses were completely removed by a depth filtration mechanism, that is, capture by nanotube bundles inside the CNT layer. Liu et al. [44] also reported that the adsorption process of virus on CNTs follows the chemical adsorption mechanism and the process may be associated with electronic sharing or electronic exchange of covalent forces in the surface between nanomaterials and virus. The removal rate of virus became higher with the dosage of nanomaterial since the total adsorption effect is boosted as the dosage increases. In this study, Fig. 10 shows that mechanical damage due to puncture and straining by CNTs can be inferred as one of virus removal mechanisms.

In this paper, we introduced a methodology that CNT air filter can be fabricated by coating aerosolized CNTs on a filter at atmospheric pressure and room temperature condition. Conventionally, wet coating by solution process has been used to deposit any functional materials to a filter, followed by a drying process with heated air flow. CNT air filter also can be fabricated by CNT growth on a filter medium via CVD process [33], where a tube furnace need to be used. However, using heated air flow or tube furnace often causes deformation of filter materials. Since our methodology does not include any solution process and high temperature treatment on the filter, possible chances of filter deformation are avoided.

In this paper, CNT air filter was fabricated in a laboratory scale. If we want to scale up the fabrication process, we need to supply higher amount of CNTs, use a nozzle with bigger diameter, and increase the number of nozzles to cover large area deposition, and so on. CNT air filter can be used in a wide range of applications such as automobile air conditioning system, secondary sterilization system, and counter-terrorism mask.

4. Concluding remarks

This study is the first to report the fabrication of CNT filters at atmospheric pressure and room temperature using electro-aerodynamic deposition of aerosolized CNTs. CNT filters had better filtration efficiencies for aerosolized bacteriophage MS2 than medium air filters with a negligible decrease in pressure. The particle filtration efficiency was increased to 33.3% in the most penetration particle size zone (100 nm) and the antiviral efficiency of the CNT filter was 92% when the coating areal density was 1.5×10^9 #/cm^2. The susceptibility constant of virus to CNTs was 0.2 cm^2/μg. These CNT filters will be useful for both filtration and inactivation of viral aerosols.

Acknowledgement

This research is supported by Korean Ministry of Environment as “The Eco-Innovation project” (402-111-005).

Appendix A. Supplementary data

Supplementary data associated with this article can be found, in the online version, at http://dx.doi.org/10.1016/j.carbon.2014.04.019.

REFERENCES

[1] Douwes J, Thome P, Pearc N, Heederik D. Review: bioaerosol health effects and exposure assessment: progress and prospects. Ann Occup Hyg 2003;47:187–200.
[2] Fung F, Hughson WG. Health effects of indoor fungal bioaerosol exposure. J Occup Environ Hyg 2003;18:535–44.
[3] Husman T. Health effects of indoor-air microorganisms. Scand J Work Environ Health 1996;22:5–13.
[4] Booth TF, Kournikakis B, Bastien N, Ho J, Kobasa D, Stadnyk L. Review: detection of airborne sever acute respiratory syndrome (SARS) coronavirus and environmental contamination in SARS outbreak units. J Infect Dis 2005;191:1472–7.
[5] Yu TS, Li Y, Wong TW, Tam W, Chan AT, Lee JH. Evidence of airborne transmission of the severe acute respiratory syndrome virus. N Engl J Med 2004;350:1731–9.
[6] Blachere FM, Lindsley WG, Pearce TA, Anderson SE, Fisher M, Khakoo R. Measurement of airborne influenza virus in a hospital emergency department. Clin Infect Dis 2009;48:438–40.
[7] Sawyer MH, Chamberlain CJ, Wu YN, Aintablian N, Wallace MR. Detection of Varicella-Zoster virus DNA in air samples from hospital rooms. J Infect Dis 1994;169:91–4.
[8] Fabian P, McDevitt JJ, DeHaan WH, Fung RO, Cowling BJ, Chan KH. Influenza virus in human exhaled breath: an observational study. PLoS One 2008;3:e2691.
[9] Stelzer-Braid S, Oliver BG, Blazey AJ, Argent E, Newsome TP, Rawlinson WD. Exhalation of respiratory viruses by breathing, coughing, and talking. J Med Virol 2009;81(9):1674–9.
[10] Loeb M, Dafoe N, Mahony J, John M, Sarabia A, Glavin V. Surgical mask vs N95 respirator for preventing influenza among health care workers. JAMA 2009;302:1865–71.
[11] Simmons RB, Crow SA. Fungal colonization of air filters for use in heating, ventilating and air conditioning (HVAC) systems. J Ind Microbiol Biotechnol 1995;14:41–5.
[12] Ahearn DG, Crow SA, Simmons RB, Price DL, Mishra SK, Pierson DL. Fungal colonization of air filters and insulation in a multi-story office building: production of volatile organics. Curr Microbiol 1997;35:305–8.
[13] Simmons RB, Price DL, Nobel JA, Crow SA, Ahearn DG. Fungal colonization of antimicrobial filter treatments on microbial colonization of air panel filters. Am Ind Hyg Assoc J 1997;58:900–4.
[14] Verdenelli MC, Cecchini C, Orpianesi C, Dadea GM, Cresci A. Efficacy of antimicrobial filter tretments on microbial colonization of air panel filters. J Appl Microbiol 2003;94:9–15.
[15] Li J, Li M, Shen F, Zou Z, Yao M, Wu C. Characterization of biological aerosol exposure risks from automobile air conditioning system. Environ Sci Technol 2013;47:10660–6.
[16] Srivastava A, Srivastava ON, Talapatra S, Vajtai R, Ajayan PM. Carbon nanotube filters. Nat Mater 2004;3:610–4.
[17] Brady-Este'vez AS, Kang S, Elimelech M. A single walled carbon nanotube filter for removal of viral and bacterial pathogens. Small 2008;4:481–4.
[18] Brady-Este'vez AS, Nguyen TH, Gutierrez L, Elimelech M. Impact of solution chemistry on viral removal by a single-walled carbon nanotube filter. Water Res 2010;44:3773–80.
[19] Brady-Este'vez AS, Schnoor MH, Vecitis CD, Saleh NB, Elimelech M. Multiwalled carbon nanotube filter: improving viral removal at low pressure. Langmuir 2010;26:14975–82.
[20] Brady-Este'vez AS, Schnoor MH, Kang S, Elimelech M. SWNT–MWNT hybrid filter attains high viral removal and bacterial inactivation. Langmuir 2010;26:19153–8.
[21] Kang S, Mauter MS, Elimelech M. Microbial cytotoxicity of carbon-based nanomaterials: implications for river water and waste water effluent. Environ Sci Technol 2009;43:2648–53.

[22] Lee KW, Liu BYH. On the minimum efficiency and the most penetrating particle size for fibrous filters. J Air Pollut Control Assoc 1980;30(4):377–81.
[23] Celik E, Park H, Choi H, Choi H. Carbon nanotube blended polyethersulfone membranes for fouling control in water treatment. Water Res 2011;45:274–82.
[24] Mostafavi ST, Mehrnia MR, Rashidi AM. Preparation of nanofilter from carbon nanotubes for application in virus removal from water. Desalination 2009;238:271–80.
[25] Rahaman SM, Vecitis CD, Elimelech M. Electrochemical carbon nanotube filter performance toward virus removal and inactivation in the presence of natural organic matter. Environ Sci Technol 2012;46:1556–64.
[26] Vecitis CD, Schnoor MH, Rahaman MS, Schiffman JD, Elimelech M. Electrochemical multiwalled carbon nanotube filter for viral and bacterial removal and inactivation. Environ Sci Technol 2011;45:3672–9.
[27] Viswanathan G, Kane DB, Lipowicz PJ. High efficiency fine particulate filtration using carbon nanotube coatings. Adv Mater 2004;16:2045–9.
[28] Park SJ, Lee DG. Development of CNT-metal-filters by direct growth of carbon nanotubes. Curr Appl Phys 2006;6(S1):e182–6.
[29] Karwa AN, Tatarchuk BJ. Aerosol filtration enhancement using carbon nanostructures synthesized within a sintered nickel microfibrous matrix. Sep Purif Technol 2012;87:84–94.
[30] Yildiz O, Bradford PD. Aligned carbon nanotube sheet high efficiency particulate air filters. Carbon 2013;64:295–304.
[31] Guan T, Yao M. Use of carbon nanotubes filter in removing bioaerosols. J Aerosol Sci 2010;41:611–20.
[32] Xu Z, Yao M. Effects of single-walled carbon nanotube filter on culturability and diversity of environmental bioaerosols. J Aerosol Sci 2011;42:387–96.
[33] Park JH, Yoon KY, Na H, Kim YS, Hwang J, Kim J, et al. Fabrication of a multi-walled carbon nanotube-deposited glass fiber air filter for the enhancement of nano and submicron aerosol particle filtration and additional antibacterial efficacy. Sci Total Environ 2011;409:4132–8.
[34] Park J, Jeong J, Kim C, Hwang J. Deposition of charged aerosol particles on a substrate by collimating through an electric field assisted coaxial flow nozzle. Aerosol Sci Technol 2013;47:512–9.
[35] Yoon KY, Byeon JH, Park JH, Hwang J. Susceptibility constants of *Escherichia coli* and *Bacillus subtilis* to silver and copper nanoparticles. Sci Total Environ 2007;373:572–5.
[36] Kim YS, Yoon KY, Park JH, Hwang J. Application of air ions for bacterial de-colonization in air filters contaminated by aerosolized bacteria. Sci Total Environ 2011;409:748–55.
[37] Park J, Kim C, Jeong J, Lee SG, Hwang J. Design and evaluation of a unipolar aerosol charger to generate highly charged micron-sized aerosol particles. J Electrost 2011;69:126–32.
[38] Park D, An M, Hwang J. Development and performance test of a unipolar diffusion charger for real-time measurements of submicron aerosol particles having a log-normal size distribution. J Aerosol Sci 2007;38:420–30.
[39] Kim C, Noh KC, Hwang J. Numerical investigation of corona plasma region in negative wire-to-duct corona discharge. Aerosol Air Qual Res 2010;10:446–55.
[40] Hinds WC. Aerosol technology: properties, behavior, and measurement of airborne particle. 2nd ed. New York: Wiley-Interscience; 1999.
[41] Jones TB. Electromechnics of particles. New York: Cambridge University Press; 1995.
[42] Keblinski P, Nayak SK, Zapol P, Ajayan PM. Charge distribution and stability of charged carbon nanotubes. Phys Rev Lett 2002;89:255503-1–4.
[43] Davies CN. Air filtration. London: Academic Press; 1973.
[44] Liu S, Zheng X, Yang T, Liu J, Li J. The removal and inhibitory effect of CNTs on model viruses. Mater Sci Forum 2013;743–744:402–8.